JEECS (Journal of Electrical Engineering and Computer Sciences)
Vol. 11, No. 2, December 2026, pp. 151-160
e-ISSN: 2579-5392 p-ISSN: 2528-0260

Body Mass Index Estimation Based on Height and Weight Using Image Processing

Muhammad Muchlis Abimanyu, Anindita Septiarini, Masna Wati, Andi Tejawati

Program Studi Informatika, Universitas Mulawarman, Jl. Sambaliung No. 9, Samarinda, Kalimantan Timur, 75119, Indonesia

Article Info

Article history:
Received: 18 May 2026
Revised: 2 August 2026
Accepted: 8 August 2026

Keyword:
Body mass index
Image processing
Height estimation
U²-Net
Weight estimation

Abstract

Body Mass Index (BMI) is a widely used indicator for evaluating body proportions and individual health status. Traditional measurement methods require direct physical contact and are time-consuming. Previous studies have utilized image-based BMI measurement using controlled backgrounds. However, this limitation restricts their application in real-world settings. Moreover, no studies have combined background-independent segmentation with a camera-parameter-based conversion from pixels to physical units, leaving accurate, background-agnostic BMI estimation an open problem. This research addresses this gap using digital image processing on front-view and side-view human body images. The proposed methods include body segmentation using the U^2-Net deep learning model, height estimation using pinhole camera projection approach that accounts for camera parameters (focal length, sensor size, camera distance), and weight estimation based on body volume modeling using an elliptical tube slice geometry. The body is treated as a stack of elliptical cross-sections whose width and depth are read from the front- and side-view silhouettes and summed into a total volume. Calibration and correction factors were determined through numerical optimization to obtain optimal global values. The dataset consists of 120 body images collected from 20 subjects. Experimental results show that the system achieves an accuracy of 96.2% (MAE 6.0 cm, RMSE 7.6 cm, MAPE 3.8%) for height estimation and 82.3% (MAE 9.7 kg, RMSE 13.2 kg, MAPE 17.7%) for weight estimation. BMI category classification accuracy reaches 60%. The use of U^2-Net enables body segmentation without requiring a controlled background, making the system more flexible and applicable for real-world environments.

Corresponding author:
Anindita Septiarini, aninditaseptiarini@gmail.com
DOI: https://doi.org/10.54732/jeecs.v11i2.5

1. Introduction

Physical health is an important aspect that affects the quality of life. Body proportions that are not ideal, whether due to excess or insufficient body weight, can increase the risk of chronic diseases such as hypertension, type 2 diabetes, and heart disease [1], [2]. One commonly used method to assess body proportion is the Body Mass Index (BMI), which is calculated as the ratio of body weight to the square of height [3]. Conventional BMI measurement requires manual measurement using a measuring tape and scales. This approach requires direct physical contact, is time-consuming, and is prone to measurement errors such as parallax error, improper body position, and instrument limitations [4]. With the advancement of image processing and computer vision technology, opportunities have emerged to develop more practical, automated, and contactless BMI estimation methods [5].

Various studies have developed image-based BMI estimation using different approaches. Ref [5] developed a system based on computer vision using linear regression and achieved an accuracy of 98.96%

for height, 88.54% for weight, and 88.24% for BMI. Meanwhile, [6] proposed a Body Surface Area (BSA) approach from front-view images, achieving high accuracy of 99.15% for height and 97.35% for weight. Another approach was carried out by [7] using Morphological Image Processing to extract body shape features, achieving height and weight accuracy of 98.42% and 94.4%, respectively; using wireless sensing-based BMI estimation and Deep Residual Network (ResNet-50) achieved an F1 score of 73.66% [8]. These approaches demonstrate that image-based BMI estimation has high potential, although each method still has limitations in practical application.

However, the primary limitation of this prior research is its dependence on specific backgrounds such as white or green screen for segmentation, limiting flexibility in real-world environments [5], [6]. This research proposes a different approach using the U²-Net deep learning model for salient object segmentation, which does not rely on specific background conditions. Additionally, this research uses a camera projection approach for height estimation that considers camera parameters more accurately, along with three-dimensional geometry modeling based on two viewpoints for body volume estimation.

This research aims to implement and evaluate an image-based BMI estimation system capable of operating under diverse background conditions. The system is designed using U²-Net segmentation, camera projection-based height estimation, and elliptical tube volume geometry-based weight estimation, with calibration factors determined through numerical optimization. The system is tested on 120 front-view and side-view images from 20 subjects with manually measured height and weight as ground truth, and its performance is evaluated using MAE, RMSE, and MAPE for height and weight, together with category-level agreement against the WHO BMI classification.

2. Research Methodology

This research is designed within a systematic framework encompassing a series of structured stages, from body image data acquisition to performance evaluation of the BMI estimation system. The overall system workflow consists of three interconnected core components: body silhouette segmentation using the U²-Net deep learning model, camera projection-based height estimation, and weight estimation through body volume geometry modeling. The entire process is implemented in Python using ONNX Runtime for model inference, OpenCV for image processing, NumPy for numerical computation, and Matplotlib for result visualization. The overall system block diagram is shown in Figure 1.

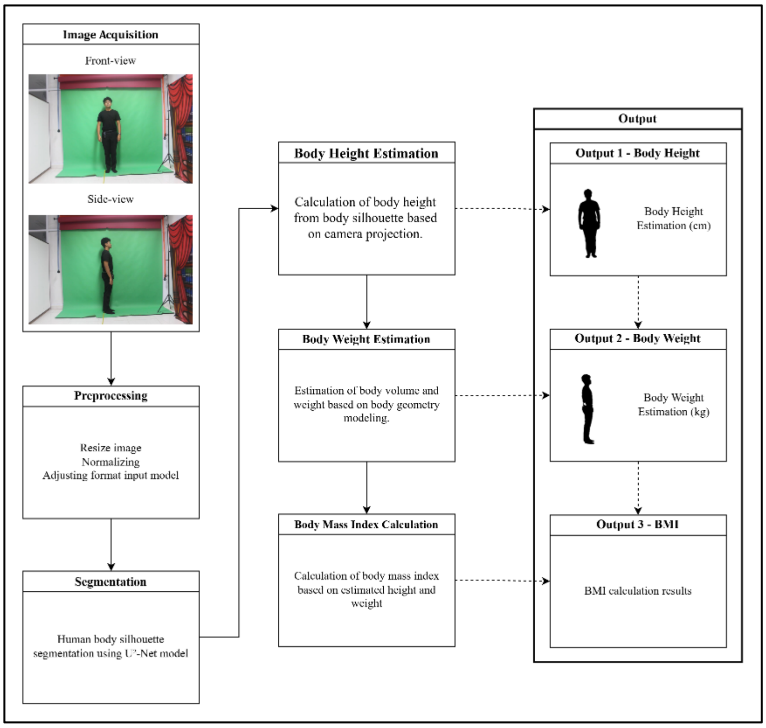

Figure 1. Overall System Design Process

2.1. Image Acquisition

Image acquisition was performed using a Canon EOS Kiss X7 camera with a Canon EFS 18–55 mm lens at a focal length of 18 mm. Images were captured from a distance of 360 cm between the camera and the subject, with the camera positioned at a height of 100 cm from the floor. The original image resolution was 5184 × 3456 pixels in CR2/JPG format.

The dataset consists of 120 images, comprising 60 front-view images and 60 side-view images from 20 subjects. Each subject was photographed under three different conditions to simulate posture variations in real-world scenarios. Height and weight of each subject were manually measured using a measuring tape and digital scales as ground truth data. Ground-truth height ranged from 144 to 183 cm and weight ranged from 42.6 to 83.5 kg, giving an actual BMI range of 17.3 to 29.4 kg/m^2, which under the WHO classification in Table 1 corresponds to 1 underweight, 15 normal-weight, and 4 overweight subjects. Images were captured against unconstrained, non-uniform backgrounds rather than a plain or green-screen backdrop, so that the test scenario reflects the flexible, background-agnostic condition the system is designed for

2.2. Preprocessing

The preprocessing stage prepares images to match the input format required by the U^2-Net model. The process includes resizing images to 320×320 pixels, normalizing pixel values to the range 0–1, and adjusting to the channel-first (CHW) format with an added batch dimension.

2.3. Segmentation

U^2-Net is a deep learning architecture based on convolutional neural networks (CNN) designed for salient object detection—the identification and segmentation of the most prominent objects in an image [9]. CNN is widely used in computer vision tasks such as classification and segmentation due to its ability to hierarchically extract spatial features through convolution operations [10]. The model adopts a nested encoder-decoder structure capable of capturing both global context and local detail at various scales.

Inference is performed using ONNX Runtime. The model output is a probability mask that is subsequently converted into a black-and-white binary silhouette through thresholding. The U^2-Net model used is a pre-trained model applied directly for inference without additional training.

2.4. Height Estimation

Height estimation uses the pinhole camera projection model, which describes the mapping of points from three-dimensional space to the two-dimensional camera sensor plane [11]. The body height derived from segmentation is initially in pixel units and must be converted to centimeters (cm). Because Equation (1) is a direct proportion, the estimated height increases with the silhouette height in pixels and with the camera-to-object distance, and decreases as the focal length increases; consequently, an error in measuring the camera-to-object distance or in the segmented silhouette height propagates linearly into the height estimate, which motivates the calibration step in Equation (2).

The conversion is performed in two stages: first, object height in pixels is converted to sensor-plane size; second, the sensor size is projected to real-world size using pinhole geometry parameters (focal length and camera-to-object distance). With assumptions that the camera is perpendicular to the subject, there is no positional offset, and only vertical projection is considered, the relationship is expressed as Equation (1):

$$H_{real} = \frac{h_{px}}{res_v} \times \frac{sensor_h}{f} \times d \tag{1}$$

H_{real} is the actual object height (cm), h_{px} is the silhouette height in pixels, res_v is the vertical image resolution (3456 pixels), $sensor_h$ is the camera sensor height (1.49 cm), f is the focal length (1.8 cm), and d is the camera-to-object distance (360 cm). To reduce deviation due to optical distortion and imperfect capture conditions, a calibration factor is applied as a corrective multiplier, as expressed in Equation (2):

$$H_{est} = k_h \times H_{real} \tag{2}$$

H_{est} is the calibrated estimated height (cm) and k_h is the corrective multiplier determined through numerical optimization.

2.5. Weight Estimation

Body weight is estimated through geometry modeling using front-view and side-view silhouettes. This approach represents the human body as a series of vertical elliptical tube slices stacked along the body height [12]. The volume of each slice is calculated using Equation (3):

$$V_i = a_i \times b_i \times h_i \tag{3}$$

V_i is the estimated volume of slice i (cm^3), a_i is the half-width of the front-view silhouette at row i (cm), b_i is the half-width of the side-view silhouette at row i (cm), and h_i is the height of each slice (cm). Each row of the front-view silhouette supplies the ellipse's width semi-axis and the corresponding row of the side-view silhouette supplies its depth semi-axis, so the two viewpoints jointly fix the cross-sectional shape at that height without assuming a fixed body proportion. Total body volume is obtained by summing all slice volumes from top to bottom [12]:

$$V_{total} = \sum_{i=1}^{n} \pi \times a_i \times b_i \times h_i \tag{4}$$

After obtaining the total volume, body weight is estimated by multiplying the volume by average human body density with a correction factor applied to compensate for the simplified 2D-based geometry [12], [5]:

$$W_{est} = \frac{V_{total} \times k_v \times \rho}{1000} \tag{5}$$

W_{est} is the estimated body weight (kg), k_v is the corrective volume multiplier determined through numerical optimization, and ρ is the average human body density (1 g/cm^3) [12].

In Equation (5), density converts the raw geometric volume to a raw mass, while the correction factor separately compensates for the elliptical-tube model overestimating volume relative to the true body contour; the two terms are multiplicative, so a fixed percentage error in the segmented silhouette area propagates as the same percentage error in the final weight estimate.

2.6. Determination of Calibration and Correction Factors

The height calibration factor and volume correction factor are determined through numerical optimization. Numerical optimization is a mathematical technique that finds optimal parameter values by minimizing a defined objective function iteratively [13], as expressed in Equation (6):

$$minimize \sum_{i=1}^{n} (|H_{est_i} \times H_{actual_i}| + |W_{est_i} \times W_{actual_i}|) \tag{6}$$

Optimization is performed for each front-view and side-view image pair. Each subject has three image pairs, yielding three calibration factors and three correction factors per subject. These three values are averaged to obtain one representative value per subject, and all subject representative values are then averaged again to produce one global calibration factor and one global correction factor used consistently throughout system testing.

2.7. Performance Evaluation

System performance is evaluated using Mean Absolute Error (MAE) and Mean Absolute Percentage Error (MAPE). MAE measures the average absolute difference between estimated and actual values, while MAPE expresses the error as a relative percentage of the actual value [14]. In addition, Root Mean Square Error (RMSE) is reported, which squares each deviation before averaging and therefore penalizes large individual deviations more heavily than MAE; reporting RMSE alongside MAE and MAPE indicates whether error is spread evenly across subjects or concentrated in a few outliers. System accuracy is expressed as 100% − MAPE. BMI category evaluation is also performed by comparing estimated categories with actual BMI categories based on the World Health Organization (WHO) standard [2], as shown in Table 1.

Table 1. WHO BMI Category Classification

Category	BMI Range (kg/m^2)
Underweight	< 18.5
Normal	18.5 – 24.9
Overweight	25.0 – 29.9
Obese Class I	30.0 – 34.9
Obese Class II	35.0 – 39.9

3. Results and Discussions

3.1. Body Segmentation Using U²-Net

The U²-Net model successfully separated human body silhouettes from the background in both front-view and side-view images. The generated segmentation masks clearly delineated the body area, and after thresholding, binary silhouettes suitable for body dimension estimation were produced. Under certain conditions, segmentation results were influenced by clothing type, shadow presence, and subject posture variations; however, the generated silhouettes remained adequate for the overall estimation process. Examples of body segmentation results using U²-Net are shown in Figure 2.

3.2. Calibration and Correction Factor Determination

The height calibration factor and body volume correction factor were determined using numerical optimization on all image pairs. Optimal values from each image were averaged per subject to obtain global factors used consistently across all data, as shown in Table 2.

The global calibration factor of 0.8668 indicates that the pixel-to-centimeter height conversion consistently overestimates actual height and requires a corrective reduction. The inter-subject variation (0.8289–0.9709) reflects individual differences in posture and image capture conditions. The global volume correction factor of 0.5520 indicates that geometric body volume estimates are consistently larger than actual volumes, which is expected since the elliptical model does not account for body curvature and contour detail.

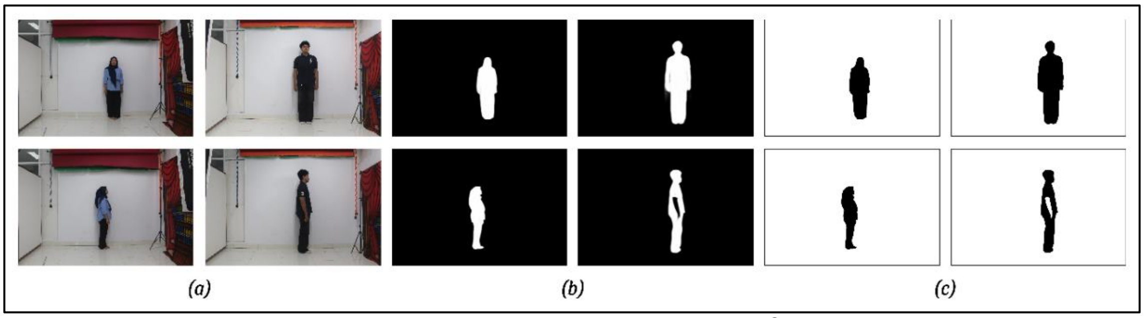

Figure 2. Body Segmentation Results Using U²-Net:
(a) Original front-view and side-view images; (b) Segmentation mask output of U²-Net; (c) Binary silhouette after mask thresholding

Table 2. Calibration and Correction Factor Values per Subject

Subject	Height Calibration Factor	Volume Correction Factor
S1	0.9556	0.4951
S2	0.9098	0.8574
S3	0.9709	0.4857
S4	0.9225	0.4755
S5	0.8572	0.6357
S6	0.8687	0.5686
S7	0.8582	0.6820
S8	0.8802	0.4977
S9	0.8424	0.6736
S10	0.8597	0.5768
S11	0.8490	0.5984
S12	0.8567	0.5381
S13	0.8289	0.4876
S14	0.8483	0.5222
S15	0.8373	0.4980
S16	0.8320	0.5702
S17	0.8382	0.4444
S18	0.8324	0.5223
S19	0.8424	0.3568
S20	0.8460	0.5534
Global Average	0.8668	0.5520

3.3. Height Estimation Results

Height estimation was tested using the global calibration factor of 0.8668 on all data. This factor was applied uniformly across all 20 subjects and their respective image pairs, ensuring consistency in the evaluation process. The complete results, including actual height, estimated height, MAE, and MAPE for each subject, are presented in Table 3, and the corresponding RMSE is reported below.

Based on Table 3, the system achieved an average MAE of 6.0 cm and MAPE of 3.8%, equivalent to an accuracy of 96.2%. The corresponding RMSE is 7.6 cm; since RMSE is only slightly above MAE, the height error is distributed fairly evenly across subjects rather than dominated by a few extreme outliers. Most subjects showed estimates close to actual values, with MAPE below 5% for 14 out of 20 subjects. Subjects 1, 3, and 16 had MAPE values above 9%, likely due to non-erect posture during image capture. This high height accuracy is supported by the use of measured camera projection parameters and optimization-derived calibration factors.

Table 3. Height Estimation Evaluation Results

Subject	Actual (cm)	Estimated (cm)	MAE (cm)	MAPE (%)
S1	160	144.9	15.1	9.5
S2	173	165.6	7.5	4.3
S3	156	139.1	16.9	10.9
S4	150	140.4	9.6	6.4
S5	183	185.2	2.2	1.2
S6	154	154.1	0.1	0.1
S7	165	166.6	1.6	1.0
S8	170	167.5	2.5	1.5
S9	173	178.2	5.2	3.0
S10	158	159.7	1.7	1.1
S11	155	157.8	2.8	1.8
S12	164	166.0	2.0	1.2
S13	147	154.2	7.2	4.9
S14	154	157.6	3.6	2.4
S15	165	171.4	6.4	3.9
S16	148	162.6	14.6	9.8
S17	156	161.8	5.8	3.7
S18	157	163.7	6.7	4.2
S19	144	148.2	4.2	2.9
S20	157	161.0	4.0	2.6
Average			6.0	3.8

Table 4. Weight Estimation Evaluation Results

Subject	Actual (kg)	Estimated (kg)	MAE (kg)	MAPE (%)
S1	61.4	51.0	10.4	17.0
S2	72.8	40.9	31.9	43.8
S3	60.2	48.1	12.2	20.2
S4	42.7	40.2	2.5	5.9
S5	83.5	74.1	9.4	11.3
S6	63.1	65.4	2.3	3.7
S7	57.9	48.5	9.4	16.3
S8	69.3	71.3	2.0	2.9
S9	59.6	57.1	2.5	4.2
S10	65.2	65.0	0.2	0.2
S11	70.7	67.8	2.9	4.1
S12	50.4	53.4	3.0	6.0
S13	42.9	60.7	17.8	41.4
S14	51.3	57.3	6.0	11.6
S15	63.8	79.1	15.3	23.9
S16	60.5	66.4	5.9	9.7
S17	47.1	63.5	16.4	34.8
S18	42.6	51.2	8.6	20.1
S19	45.8	78.0	32.2	70.2
S20	48.2	51.8	3.6	7.6
Average			9.7	17.7

3.4. Weight Estimation Results

Weight estimation was tested using the global correction factor of 0.5520 on all data. Table 4 presents a comparison of actual and estimated body weights for each subject, and the corresponding RMSE is reported below.

Weight estimation achieved an average MAE of 9.7 kg and MAPE of 17.7%, equivalent to an accuracy of 82.3%. The corresponding RMSE is 13.2 kg, noticeably higher than the MAE; because RMSE penalizes large deviations more heavily than MAE, this gap indicates that weight error is concentrated in a small number of subjects rather than spread evenly, consistent with the wide MAPE range below. Weight estimation exhibited higher variability than height estimation, with MAPE ranging from 0.2% to 70.2%. Subjects 2, 13, and 19 had the highest errors, attributed to posture and clothing types that are poorly represented by the simple elliptical model.

The higher complexity of weight estimation is caused by several factors: (1) the high variability of human body shapes cannot be fully captured by elliptical tube slices; (2) small segmentation errors have a large impact on volume calculations; (3) clothing type affects silhouette width and thus volume estimation; (4) a single global correction factor cannot accommodate individual differences.

3.5. Body Mass Index Classification Results

BMI values were computed from estimated height and weight, and BMI categories were determined using the WHO standard in Table 1. A comparison of actual and estimated BMI values along with category agreement is shown in Table 5.

Out of 20 subjects, 12 subjects (60%) achieved correct BMI category predictions. The lower classification accuracy compared to component estimation accuracies is due to the sensitivity of BMI to small estimation errors. Minor errors in weight or height can shift the BMI value across category thresholds, particularly for subjects whose BMI is close to a boundary.

3.6. Comparison with Related Research

The following illustrates the differences and similarities in results between the method proposed in this study and previous approaches in the field of image-based BMI estimation. Each prior method varies in terms of segmentation technique, background requirements, and achieved accuracy. A comprehensive comparison of the system's performance against similar studies is presented in Table 6.

Table 5. BMI Classification Evaluation Results

Subject	Actual BMI	Actual Category	Estimated BMI	Estimated Category	Match
S1	23.98	Normal	24.31	Normal	Yes
S2	24.33	Normal	14.92	Underweight	No
S3	24.73	Normal	24.89	Normal	Yes
S4	18.98	Normal	20.42	Normal	Yes
S5	24.95	Normal	21.58	Normal	Yes
S6	26.57	Overweight	27.45	Overweight	Yes
S7	21.28	Normal	17.48	Underweight	No
S8	23.99	Normal	25.40	Overweight	No
S9	19.91	Normal	17.99	Underweight	No
S10	26.12	Overweight	25.47	Overweight	Yes
S11	29.44	Overweight	27.22	Overweight	Yes
S12	18.74	Underweight	19.36	Normal	No
S13	19.88	Normal	25.54	Overweight	No
S14	21.63	Normal	23.03	Normal	Yes
S15	23.44	Normal	26.88	Overweight	No
S16	27.60	Overweight	25.13	Overweight	Yes
S17	19.34	Normal	24.26	Normal	Yes
S18	17.28	Underweight	19.12	Normal	No
S19	22.09	Normal	35.50	Obese Class I	No
S20	19.55	Normal	19.98	Normal	Yes

Table 6. Comparison with Related Research

Segmentation Method	Background	Height Accuracy	Weight Accuracy
Grayscale+Edge+Bbox [5]	White/Green Screen	98.96%	88.54%
Morphology [6]	White	99.15%	97.35%
Pixel Ratio [15]	Not specified	–	95.6%
GLCM+SVM+BSA [16]	Controlled	95.97%	95.39%
MIP+BSA [7]	Controlled	98.42%	94.4%
U²-Net (Deep Learning)	**Free/Flexible**	**96.2%**	**82.3%**

Table 6 shows that most prior research relied on controlled specific backgrounds to simplify segmentation, resulting in higher weight accuracy (94–97%). Although the weight accuracy of this study (82.3%) is lower than those works, its primary advantage is the flexible background-agnostic segmentation enabled by U²-Net, making it more applicable in real-world conditions. The height accuracy (96.2%) is competitive with related research, demonstrating that the proposed camera projection approach is effective for estimating linear body dimensions.

3.7. Discussions

Taken together, the results in Sections 3.3–3.6 show a consistent pattern: accuracy declines at each stage where the estimation depends on a larger number of upstream measurements. Height estimation, which depends on a single linear pixel-to-centimeter conversion, reaches 96.2% accuracy (RMSE 7.6 cm). Weight estimation, which depends on the segmented silhouette area at every row of the body, reaches 82.3% accuracy (RMSE 13.2 kg). BMI, which multiplies the errors of both height and weight together, falls to 60% category accuracy. This gradient indicates that the elliptical-tube volume model, not the U²-Net segmentation or the camera projection step, is the main bottleneck limiting overall system accuracy. Three findings support this interpretation. First, the segmentation evaluation in Section 3.1 shows the U²-Net masks closely match the manually produced ground truth, so segmentation quality alone does not explain the weight error. Second, the weight-error outliers in Section 3.4 (Subjects 2, 13, and 19) coincide with loose clothing or non-frontal posture, both of which distort the silhouette width without changing the true body volume; the elliptical-tube model has no mechanism to distinguish a wider silhouette caused by clothing from one caused by an actually larger body. Third, a single global correction factor is applied to every subject regardless of build, so subjects whose body shape departs most from an average elliptical cross-section are systematically over- or under-corrected. Recent work outside this dataset reaches a similar conclusion from a different direction: reviews of image-based anthropometry report that deep- feature and learned-regression approaches generally outperform fixed geometric body models, particularly when clothing and pose are not controlled [17], and a multiplex-network approach that fuses 2D anthropometric ratios, 3D pose-derived measurements, and deep features has been reported to lower BMI estimation error relative to single-representation methods [18]. This suggests that the geometric-only volume model used here, while background-flexible, sits at a point in the design space that trades estimation accuracy for reduced computational cost and data requirements relative to these learned approaches.

Several limitations remain unresolved by this study. The sample of 20 subjects, while sufficient to demonstrate feasibility, is too small to establish whether the global calibration and correction factors generalize to body types, clothing styles, or camera setups outside this dataset; the 0.2%–70.2% MAPE range for weight in Table 4 already shows that a single global factor performs unevenly across the present sample, and a larger and more diverse sample would be needed to confirm this. The system was also evaluated with a fixed camera distance and a single lens, so its accuracy under variable acquisition distances remains untested. Finally, because the volume model assumes an elliptical cross-section at every body height, it cannot correct for a silhouette that is widened by clothing rather than tissue, and no clothing-invariant correction is proposed here.

Returning to the gap identified in Section 1, this research set out to test whether background-independent segmentation could be combined with a camera-parameter-based conversion to produce a practical, contactless BMI estimation system. That specific gap is closed: U²-Net segmentation operated without a controlled background across all 120 images, and the camera projection approach produced height estimation accuracy (96.2%) competitive with prior work that required a controlled background. However, this does not mean the broader problem of contactless BMI estimation is solved. Weight and BMI accuracy remain below the best controlled-background results in Table 6, and the category-level accuracy of 60% is not yet sufficient for clinical use, where a one-category misclassification can affect a screening decision. The system is therefore best positioned as a low-cost, flexible screening aid rather than a replacement for manual measurement in clinical settings.

4. Conclusion

This research successfully implemented an image-based BMI estimation system utilizing U²-Net segmentation, camera projection, and elliptical tube slice geometry modeling. Testing with 120 images from 20 subjects demonstrated that the system achieves height estimation accuracy of 96.2% (RMSE 7.6 cm, MAPE 3.8%) and weight estimation accuracy of 82.3% (RMSE 13.2 kg, MAPE 17.7%). BMI category classification accuracy reached 60%.

The use of U²-Net enables body segmentation without a specific background, providing greater flexibility for real-world environments compared to prior approaches. Future research may focus on improving accuracy through additional training data, developing more complex body modeling methods, and applying individual-adaptive correction factors.

References

[1] B. N. Achsan *et al.*, "Faktor Risiko Obesitas Dengan Low Back Pain Kronis : Tinjauan Sistematik," *CoMPHI Journal: Community Medicine and Public Health of Indonesia Journal*, vol. 4, no. 3, pp. 241–248, 2024, doi: 10.37148/comphijournal.v4i3.188.

[2] I. Mulyasari, P. Afiatna, S. Maryanto, and A. N. Aryani, "Body Mass Index as Hypertension Predictor: Comparison between World Health Organization and Asia-Pacific Standard," *Amerta Nutrition*, vol. 7, no. 2SP, pp. 247–251, 2023, doi: 10.20473/amnt.v7i2SP.2023.247-251.

[3] A. Pratama and Z. Zulfahmidah, "Gambaran Indeks Massa Tubuh (IMT) pada Mahasiswa," *Indonesian Journal of Health*, vol. 2, no. 01, pp. 1–7, 2021, doi: 10.33368/inajoh.v2i1.29.

[4] M. Situmorang, "Penentuan Indeks Massa Tubuh (IMT) melalui Pengukuran Berat dan Tinggi Badan Berbasis MikrokontrolerAT89S51 dan PC," *Jurnal Teori Dan Aplikasi Fisika*, vol. 03, no. 02, pp. 102–110, 2017.

[5] A. B. Abadi, A. Fadllullah, S. Sumardi, S. Mahdi, and A. N. Juniar, "Perhitungan Indeks Massa Tubuh Less Contact Berbasis Computer Vision dan Regresi Linear," *MATRIK : Jurnal Manajemen, Teknik Informatika dan Rekayasa Komputer*, vol. 21, no. 3, pp. 629–638, 2022, doi: 10.30812/matrik.v21i3.1512.

[6] N. Umy Habibah, P. A. Rosyady, and R. P. Pribadi, "Analisis Indeks Masa Tubuh Berbasis Citra Digital Menggunakan Metode Body Surface Area," *Jetri : Jurnal Ilmiah Teknik Elektro*, vol. 20, no. 2, pp. 135–152, 2023, doi: 10.25105/jetri.v20i2.15398.

[7] S. Aulia, F. E. Satria, and R. D. Atmaja, "Sistem Pengukur Tinggi dan Berat Badan berbasis Morphological Image Processing," *ELKOMIKA: Jurnal Teknik Energi Elektrik, Teknik Telekomunikasi, & Teknik Elektronika*, vol. 6, no. 2, p. 219, 2018, doi: 10.26760/elkomika.v6i2.219.

[8] L. Fu, Y. Zhao, H. Chen, L. Ge, Y. Lu, and H. Zhang, "A survey on large-scale unobtrusive BMI estimation for public health," *High-Confidence Computing*, vol. 6, no. 3, p. 100402, Sep. 2026, doi: 10.1016/J.HCC.2026.100402.

[9] X. Qin, Z. Zhang, C. Huang, M. Dehghan, O. R. Zaiane, and M. Jagersand, "U 2 -Net : Going deeper with nested U-structure for salient object detection," *Pattern Recognition*, vol. 106, p. 107404, 2020, doi: 10.1016/j.patcog.2020.107404.

[10] M. R. Adrian, A. Albadri, and M. Pratiwi, "Model Deep Learning Berbasis Convolutional Neural Network (CNN) untuk Identifikasi Tingkat Kerusakan Jalan di Kota Dumai," *Jurnal Teknologi Komputer Dan Informasi*, vol. 13, no. 2, pp. 112–131, 2025, doi: 10.52072/jutekinf.v13i2.1816.

[11] E. Jeges, I. Kispál, and Z. Hornák, "Measuring human height using calibrated cameras," *2008 Conference on Human System Interaction, HSI 2008*, pp. 755–760, 2008, doi: 10.1109/HSI.2008.4581536.

[12] T. H. Supranata, P. S. S. Davin, D. K. Jeremy, A. E. Pratiwi, and M. Wulandari, "Body weight measurement using image processing based on body surface area and elliptical tube volume," *Proceedings of 2018 10th International Conference on Information Technology and Electrical Engineering: Smart Technology for Better Society, ICITEE 2018*, pp. 290–294, 2018, doi: 10.1109/ICITEED.2018.8534735.

[13] A. Géron, *Hands-On Machine Learning with Scikit-Learn , Keras , and TensorFlow*, 3rd ed., vol. 3rd Editio. Sebastopol, CA: O'Reilly Media, 2022.

[14] D. Chicco, M. J. Warrens, and G. Jurman, "The coefficient of determination R-squared is more informative than SMAPE , MAE , MAPE , MSE and RMSE in regression analysis evaluation," *PeerJ Computer Science*, pp. 1–24, 2021, doi: 10.7717/peerj-cs.623.

[15] F. Rahman, H. Fauzi, T. N. Azhar, N. Ayudina, and R. Dwiatmaja, "Analisa Metode Pengukuran Berat Badan Manusia Dengan Pengolahan Citra," *Teknik*, vol. 38, no. 1, p. 35, 2017, doi:

10.14710/teknik.v38i1.12663.

[16] T. R. Adiguna, I. R. Magdalena, and S. Saidah, “Sistem Deteksi Idealitas Berat Badan Secara Real Time Dengan Menggunakan Metode Gray Level Co-Occurance Matrix Dan Body Surface Area Designing of Ideality Weight Detection System in Real Time With Gray Level Co-Occurance Matrix Method and Body Surface Are,” *e-Proceeding of Engineering*, vol. 5, no. 3, pp. 5562–5570, 2018.

[17] H. Mohammedkhan, H. Fleuren, Ç. Güven, and E. Postma, “Inferring Body Measurements from 2D Images: A Comprehensive Review,” *Journal of Imaging*, vol. 11, no. 6, pp. 1–27, 2025, doi: 10.3390/jimaging11060205.

[18] A. Xu, T. Wang, T. Yang, and K. Hu, “Extracting Multi-Dimensional Features for BMI Estimation Using a Multiplex Network,” *Symmetry*, vol. 17, no. 6, pp. 1–16, 2025, doi: 10.3390/sym17060877.